A&A 487, 131–146 (2008)
DOI: 10.1051/0004-6361:200809366

Astronomy & Astrophysics

AGB stars as tracers of metallicity and mean age across M 33⋆

M.-R. L. Cioni[2,1], M. Irwin[3], A. M. N. Ferguson[1], A. McConnachie[4], B. C. Conn[5], A. Huxor[1,6], R. Ibata[7], G. Lewis[8], and N. Tanvir[9]

[1] SUPA, School of Physics, University of Edinburgh, IfA, Blackford Hill, Edinburgh EH9 3HJ, UK
e-mail: M.Cioni@herts.ac.uk
[2] Centre for Astrophysics Research, University of Hertfordshire, Hatfield AL10 9AB, UK
[3] Institute of Astronomy, University of Cambridge, Madingley Road, Cambridge CB3 0HA, UK
[4] Deptartment of Physics & Astronomy, University of Victoria, PO Box 3055, STN CSC, Victoria, BC, V8W 3P6, Canada
[5] European Southern Observatory, Alonso de Cordova 3107, Vitacura, Santiago, Chile
[6] Department of Physics, University of Bristol, Tyndall Avenue, Bristol BS8 1TL, UK
[7] Observatoire de Strasbourg, 11 rue de l'Université, 67000 Strasbourg, France
[8] Institute of Astronomy, School of Physics, A29, University of Sydney, NSW 2006, Australia
[9] Department of Physics and Astronomy, University of Leicester, Leicester LE1 7RH, UK

Received 8 January 2008 / Accepted 5 May 2008

ABSTRACT

Context. Wide-field JHK_s near-infrared observations covering an area of 1.8° × 1.8° centred on M 33 were obtained using WFCAM at UKIRT. These data show a large population of intermediate-age asymptotic giant branch (AGB) stars.
Aims. We have used both C-type and M-type AGB stars to determine spatial variations in metallicity and mean age across the galaxy.
Methods. We distinguished between C-type and M-type AGB stars from their location in the colour-magnitude diagram ($J - K_s$, K_s). The distribution of these stars is supported by a cross-identification between our sample and a catalogue of optically confirmed, long-period variable stars, as well as with the list of sources detected by Spitzer in the mid-infrared. We calculated the C/M ratio and the orientation of the galaxy in the sky, and compared the K_s magnitude distribution with theoretical distributions spanning a range of metallicities and star formation rates (SFRs).
Results. The C/M ratio surface map confirms a metallicity gradient in the galaxy corresponding to a spread in [Fe/H] = 0.6 dex with substructures in the inner and outer galaxy. Magnitude and colour variations suggest orientation and extinction effects on the galaxy disc. Maps showing the distribution of mean age and metallicity obtained from the K_s method suggest that: the outer galaxy disc/halo is metal poorer than the nuclear region and metal-rich clumps in the inner galaxy change location with time. The average outer ring and nuclear stellar population is ∼6 Gyr old while central regions are a few Gyr younger.

Key words. galaxies: individual: M 33 – stars: late-type – galaxies: stellar content – Galaxy: abundances – galaxies: structure

1. Introduction

M 33 (NGC 598 or the Triangulum galaxy) is located at about 15° from M 31 (Andromeda) and is the third brightest member of the Local Group. It is a spiral galaxy of type Sc II-III intermediate between large spirals and dwarf irregulars in the Local Group. A detailed review of studies of this galaxy until the year 1999, included, is given by van den Berg (2000). These studies concentrated on: the determination of the distance to the galaxy, the characterisation of its structural components (nucleus, disc and halo), the detection of variable stars although their numbers were far from complete, the determination of the age and metallicity of globular clusters which, contrary to the Large Magellanic Clouds clusters, formed regularly throughout time, and the spatial distribution and chemical analysis of HII regions, associations, supernova and supernova remnants. Abundance gradients were clearly detected. The only JK_s near-infrared study at the time of the resolved stellar population was that of McLean & Liu (1996) which failed to reveal the presence of a bulge but showed a clearly numerous intermediate-age component in the disc as well as in the centre of the galaxy. Their observations covered a field of 7.6′ × 7.6′ centred on M 33 and barely reached $K_s = 18$; sources fainter than $K_s = 17$ were affected by severe photometric errors and incompleteness.

A few years later Stephens & Frogel (2002) presented near-infrared diagrams as deep as $K_s = 22$ which outlined young, intermediate-age as well as old stellar populations in the very centre (22″ × 22″) of the galaxy. The outer region was explored by Davidge (2003) who confirmed that an intermediate-age population occurs well outside the young star forming disc. Wide-area optical observations were analysed by McConnachie et al. (2004) to refine the distance modulus of the galaxy using the tip of the red giant branch (RGB) method (see also Kim et al. 2002). Similar observations extending over the whole body of M 33 were analysed by Li et al. (2004). The authors computed theoretical spectral energy distributions (SEDs) for three different star formation rates (SFRs). A comparison with their observations suggests that for a constant SFR there is an age gradient between stellar populations of the central regions (10 Gyr old) and of the outer regions (7 Gyr old) with the youngest

⋆ Full Tables 1 and 2 are only available in electronic form at the CDS via anonymous ftp to cdsarc.u-strasbg.fr (130.79.128.5) or via
http://cdsweb.u-strasbg.fr/cgi-bin/qcat?J/A+A/487/131

component (5 Gyr old) in the spiral arms. An exponentially decreasing SFR equally reproduces the observations but ages are about 2 Gyr lower. The SE region of the galaxy, explored by Barker et al. (2007) using deep images from the Hubble Space Telescope, shows that the mean age increases from 6 (inner) to 8 (outer) Gyr assuming that star formation began 14 Gyr ago. This result was obtained from observations of three fields located within 20′−30′ from the nucleus. On the contrary, Li et al. (2004), by observing the entire galaxy, found a decrease in the age of the stellar population from the central to the outer regions. Spiral arms, however, appear younger than the outer galaxy. Block et al. (2004) obtained deep 2MASS near-infrared photometry across the whole galaxy suggesting that carbon stars delineate arcs which are the signature of accretion of low metallicity gas in the outer disc. Recent spectra confirm the existence of a few C stars at this location (Block et al. 2007). However, these arcs were not found by Rowe et al. (2005) who obtained wide-area observations in *VI* broad-band filters but also in narrow-band filters, distinguishing between C- and M-type asymptotic giant branch (AGB) stars and investigated the metallicity gradient via the C/M ratio. These authors suggest that the arcs are simply an extension of the M 33 disc.

The present work aims to recover the spatially resolved metallicity and mean age of the stellar population of M 33 by interpreting the observed K_s band distribution of AGB stars from new wide-field near-infrared data. Section 2 describes the observations and the data reduction while Sect. 3 concentrates on the analysis of the data: the comparison with theoretical distributions and the production of final maps showing the distribution of mean age and metallicity across the galaxy. Section 4 compares the results with the information available from the literature while Sect. 5 concludes this paper.

2. Observations and data reduction

The observations of M 33 were obtained as part of a program to survey the luminous red stellar populations of the Local Group galaxies using the Wide-Field CAMera (WFCAM) on the 3.8 m United Kingdom InfraRed Telescope (UKIRT) in Hawaii. WFCAM utilises 4 Rockwell Hawaii-II (HgCdTe 2048 × 2048) arrays, such that 4 separately pointed observations can be tiled together to cover a filled square of sky (a tile) of 0.75 deg^2 with 0.4″ pixels. A mosaic of 4 tiles was obtained in three broad-band filters (J, H and K_s; Tokunaga et al. 2002) covering a 3 deg^2 of sky centred on M 33. Observations in the J band were obtained using a 5 point jitter mode, using 10 s × 3 coaveraged exposures at each position, without microstepping[1], to give a total exposure time of 150 s per pointing. For the H and K_s band images a 3 point jitter with 10 s per position and a 3 × 3 microstepping was used, effectively giving 270 s total exposure per pointing.

Target frames of M 33 were acquired throughout the semester on September 29th and 30th, October 24th, November 5th and December 16th 2005, and were processed, together with the rest of the WFCAM data for those nights, using the WFCAM pipeline provided by the Cambridge Astronomy Survey Unit (http://casu.ast.cam.ac.uk/). The pipeline performs all the standard near-infrared reduction steps for instrumental signature removal: dark-correction, flatfielding, crosstalk removal, sky-correction, and systematic noise removal, all at the frame level. In addition frames forming part of a dither or interleave sequence are co-aligned and stacked/and or interleaved prior to performing source extraction. After source extraction the pipeline then produces object morphological classifications from which assorted quality control measures are computed, and also does full astrometric and photometric calibration based on the 2MASS point source catalogue (see Irwin et al. 2004; and the CASU web pages for more details). The quality control measures are used to monitor parameters such as sky brightness, seeing, limiting depth etc., and are used to select the best set of frames for further post-pipeline analysis.

In the case of M 33, since the average seeing on the frames varied between ≈0.7−1.1 arcsec, the H and K_s stacked interleaved images were subsequently resampled using 2 × 2 binning to form images with a resolution of 0.267″/pix, which is better matched to the seeing and helps to minimise the effects of seeing variations in the 3 × 3 interleaved stacked data. Source extraction and calibration were then re-run on the resampled images to give the final object catalogues per pass band, again calibrated with respect to 2MASS (Skrutski et al. 2006).

The J, H, and K_s object catalogues were then matched across the different passbands on a per pointing basis. To be considered a good match, objects had to align to better than 1″. This is significantly worse than the average positional match error between the same object in the different passbands which is better than 100 mas. The band-merged products for all pointings were then simply "glued" together to make the first pass large area complete catalogue. Duplicate entries in this catalogue, due to the overlap between pointings within a tile and between tiles, were then removed using the photometic flux error combined with the morphological classification to choose a unique "best" entry per object. This unique catalogue forms the basis for all subsequent analysis. We note that the accuracy of the 2MASS photometric calibration of 1−2% (e.g. Hodgkin et al. 2007) greatly simplifies the process.

The observing conditions corresponded to an average seeing of 1.07 ± 0.06″ which, combined with the photon-noise limited science products, allowed us to reach magnitudes of $J = 19.30 \pm 0.18$, $H = 18.70 \pm 0.12$ and $K = 18.32 \pm 0.10$ with a signal:to:noise better than 10:1 in all wavebands. We discuss completeness and crowding issues separately in Sect. 3.3.

3. Analysis and results

The first step in the data analysis was to select from the catalogue only stellar and probably stellar objects, from a pipeline stellarity index, in both J and K_s bands. No selection was performed on the H band but it is unlikely that an object will look like a star in two but not in three bands. A total of 60367 objects satisfy this selection criterion (are within 1−2σ of the stellar locus). Their histogram is shown in Fig. 1 where the dip at $K_s = 18.15$ corresponds to the discontinuity marking the transition between RGB and AGB stars. RGB stars reach their brightest magnitude at the tip of the RGB when He burning begins in their core. It is interesting to note that this dip is also present in the distribution of all sources in the catalogue for both the K_s and J band. The latter occurs at $J = 19.15$, but it is not clearly visible for stellar-like objects. The difference between the position of the dip in the two wave bands corresponds to the difference between the tip of the RGB position observed, in the same wave-bands, for the Magellanic Clouds (Cioni et al. 2000). In general, using the calibrations by Bellazzini et al. (2004) this difference depends on the total metallicity of the galaxy and for [M/H] ∼ −0.75

[1] Microstepping is used to attempt to recover some of the lost resolution due to under sampling good seeing conditions with the 0.4″ pixels. The microstepped frames are interwoven at the pixel level to give, in this case, an effective sampling of 0.133″ per interleaved pixel.

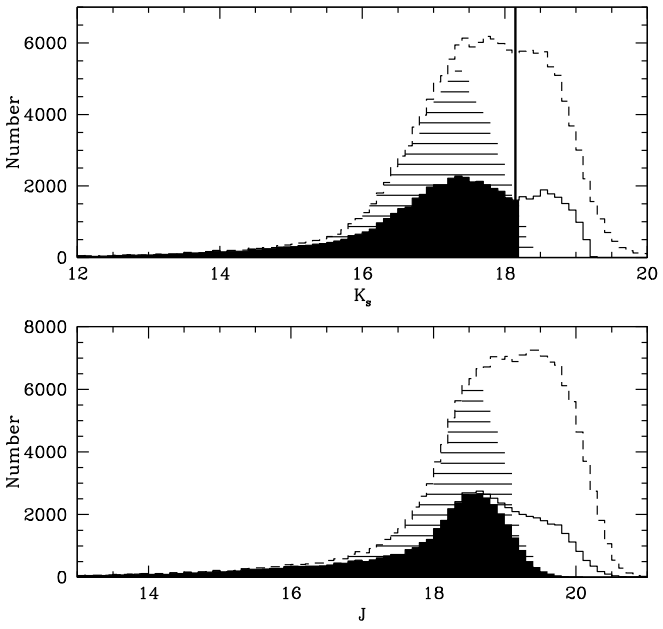

Fig. 1. Distribution of all sources listed in the catalogue as a function of magnitude (*dashed-line histogram*), those with a photometric accuracy better than 10% (*dashed-filled histogram*) and of selected stellar as well as probably stellar objects (*continuous histogram*). K_s magnitudes are shown on *the top panel* and J magnitudes on the *bottom* one. Bins correspond to 0.1 mag and magnitudes are apparent. The vertical line at $K_s = 18.15$ indicates the position of the tip of the RGB while the *continuous-filled* histograms show sources with $K_s < 18.15$, most of them are AGB stars, and their corresponding J band distribution; this is the sample used in the paper.

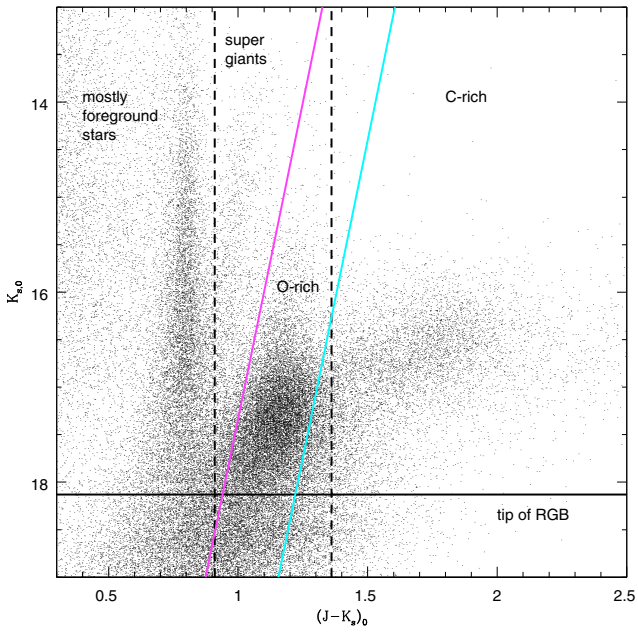

Fig. 2. Colour-magnitude diagram of the stellar sources detected in J and K_s across M 33. Dashed *vertical-lines* and continuous *slanted-lines* define regions occupied by O-rich and C-rich candidate AGB stars, respectively. These appear statistically distinct from foreground stars and super giant stars of M 33. The position of the tip of the RGB is also indicated.

(McConnachie et al. 2004) it is ∼1.1 mag, in agreement with what is observed.

The sample analyzed in this paper, for which a detailed selection is presented in the next section, contains only sources brighter than the tip of the RGB in the K_s band. Figure 1 shows that all these objects, with $K_s < 18.15$, have a photometric accuracy better than 10% in both the J and K_s bands (filled histograms). These data were then dereddened for galactic foreground extinction assuming $E(B-V) = 0.07$ (van den Bergh 2000) and adopting the reddening law from Glass et al. (2003) which gives absorptions of: $J = 0.06$, $H = 0.04$ and $K_s = 0.02$ mag.

3.1. Selection of AGB stars

Intermediate-age AGB stars are brighter than the tip of the RGB. In the near-infrared colour-magnitude diagram, $(J-K_s)_0$, $K_{s,0}$, they occupy two statistically distinct branches depending on their spectral type. C-rich, or C-type, AGB stars span a wide range of $(J-K_s)_0$ colours at an approximately constant $K_{s,0}$ magnitude because of the absorption effect of molecules such as CN and C_2. O-rich, or M-type, AGB stars span a narrow range of $(J-K_s)_0$ colours, but a large range of $K_{s,0}$ magnitudes. They define a bright extension of the RGB branch. The atmospheres of O-rich AGB stars is also dominated by molecular absorption but in this case these are mostly of H_2O, TiO and VO. Foreground stars, mostly dwarfs, observed towards M 33 are distributed in a vertical sequence at $(J-K_s)_0 \sim 0.91$ while super giant stars, belonging to M 33, define a slanted branch between foreground stars and O-rich AGB stars. Figure 2 shows the location of the different types of stars; this diagram probably includes also upper main-sequence stars as well as Cepheid variable stars which have $(J-K_s)_0$ colours bluer than AGB stars and cannot be disentangled from foreground stars using single epoch near-infrared photometry.

Two different statistical criteria can be adopted to distinguish between C-rich and O-rich AGB stars brighter than the tip of the RGB. The first criterion (using *vertical-lines*) assumes that C-rich AGB stars are redder than $(J-K_s)_0 = 1.36$ which is a visually estimated colour, chosen specifically for this galaxy, marking the departure of the reddest stellar branch from the vertical one (Fig. 2). O-rich stars, including AGB stars and super giant stars, are bluer than this colour but redder than $(J-K_s)_0 = 0.91$ which disentangles them from foreground stars. This criterion, although being subjective, relies on spectroscopic identifications of C-rich and O-rich AGB stars (Cioni et al. 2001). It has the advantage of isolating the bulk of the C star population producing a reliable but not complete sample of C-rich AGB stars. In fact, faint C stars together with super giant stars contaminate the region populated by O-rich AGB stars producing a sample, of O-rich AGB stars, which is complete but less reliable at bright and faint magnitudes. The second criterion adopts *slanted-lines*, instead of vertical lines, that better represent the inclination of the O-rich AGB branch as well as that of the RGB branch. The equations of the lines are: $K_{s,0} = -13.333(J-K_s)_0 + 30.666$ and $K_{s,0} = -13.333(J-K_s)_0 + 26.933$. O-rich AGB stars are included within these lines while C-rich AGB stars are redder (Fig. 2). The width of the region occupied by AGB stars (0.28 mag) excludes super giant stars and accounts for a possible high metallicity spread within the galaxy. This criterion was established as a result of simulating the distribution of AGB stars in the near-infrared colour-magnitude diagram (Cioni et al. 2006a). It has

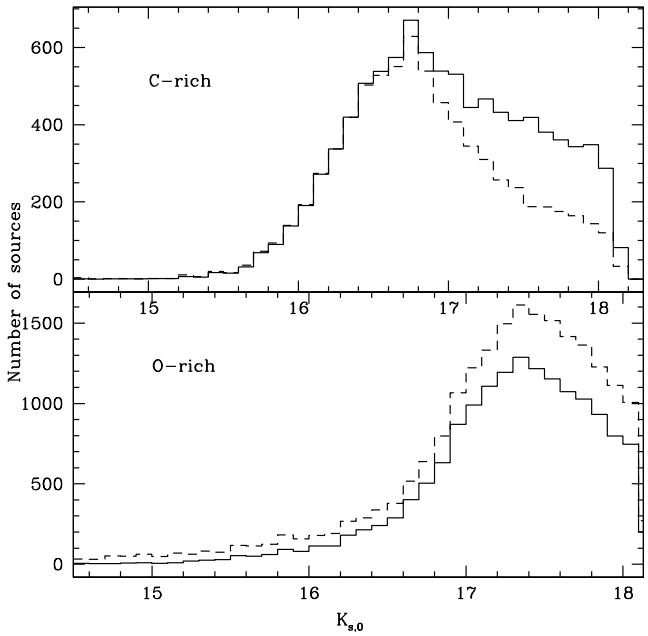

Fig. 3. Distribution of the number of C-rich and O-rich AGB stars versus $K_{s,0}$ magnitude. Both the result of selecting these stars using vertical lines (*dashed-line histograms*) and using slanted lines (*continuous-line histograms*) are shown; bins are of 0.1 mag.

the advantage of isolating the bulk of the O-rich AGB population by removing the contamination by super giant and faint C stars. The isolated sample of C stars approaches completeness although contamination around the dividing lines is not excluded at the expenses of reliability. Both criteria will be used throughout the paper as a comparison and a validation of the procedures as well as to assess uncertainties in the resulting distribution of mean age and metallicity across the galaxy.

The histograms of AGB stars selected from the near-infrared colour-magnitude diagram are shown in Fig. 3. C-rich AGB stars brighter than $K_{s,0} = 16.6$ are equally recovered by both selection criteria, while using slanted lines more fainter C-rich AGB star candidates are obtained than by using vertical lines. The C/M ratio derived from this selection is 0.60. In low-metallicity environments C-rich AGB stars are more numerous and extend to faint magnitudes. Therefore, it is possible that in M 33 there are more faint C-rich AGB stars than those occupying only the red branch. The *vertical-lines* selection criterion selects more O-rich AGB stars, however, their distribution as function of K_s magnitude is very similar to the one obtained using the slanted-lines criterion. The latter includes super giant stars and gives a C/M ratio of 0.35.

3.2. Surface distributions

The selection of a pure sample of C and M stars is a delicate task. In the previous section two criteria, commonly used in the literature, are presented and a comparison of the respective samples is briefly discussed but see also Sect. 3.3.

Battinelli et al. (2007) have recently assessed the selection of C and M stars at infrared wavelengths. Their main conclusion is that the constant $(J - K_s)$ colour discriminating between the two types of AGB stars depends on the observed stellar population. This results confirms previous evidences based on the study of the Magellanic Clouds and NGC 6822 galaxies (Cioni & Habing 2003; Cioni et al. 2005). In these cases the dividing colour is a visual estimate of the departing of the C stars branch to red colours from the almost vertical branch of M stars. The different colour used for each galaxy is attributed to the different metal content among them, although a direct calibration is not yet available. However, a subsequent study of the Magellanic Clouds has shown very good agreement between the metallicity estimated from the C/M ratio and from the K_s band magnitude distribution. There, the selection of C and M stars was made using *slanted* instead of *vertical* lines that combine the visual departure of the C stars branch to red colours and the location of C and M stars from stellar evolution models. The agreement between the metallicity distributions across each galaxy supports the evidence that the selection of C and M stars depends on environment.

What is the distribution of the bulk of C, M, super giant and foreground stars that may affect the selection criteria discussed so far? The distribution of these stars isolated from the colour-magnitude diagram is shown in Fig. 4. C stars have been selected using the *vertical-lines* criterion; M stars using the *slanted-lines* criterion; super giant stars have $(J - K_s)_0 > 0.91$, $K_{s,0} < -13.333 * (J - K_s)_0 + 30.666$ and $K_{s,0} < 17$ and foreground stars have $0.61 < (J - K_s)_0 < 0.91$ and $K_{s,0} < 17$. The sample of both super giant and foreground stars have been limited to stars much brighter than the tip of the RGB to avoid as much as possible the contamination with other stars. Maps in Fig. 4 have been obtained applying a box car smoothing to the number density calculated using bins of 1.2′.

C and M stars are both broadly and asymmetrically distributed across the galaxy and show hints of the galaxy spiral arms. Towards the centre, C stars increase in number following a broad circular structure while M stars show a well defined concentration at the location of the galaxy nucleus surrounded by a smoother elongated lower density structure. Super giant stars describe a clumpy distribution which is predominantly confined in the central region of the galaxy. Their number is considerably lower than that of C or M stars at these distance from the centre. Therefore, the C/M ratio and the analysis of the K_s magnitude distribution that follows will not be affected by the presence of super giant stars. Foreground stars are, as expected, more or less homogeneously distributed within the entire area surveyed in the direction of the M 33 galaxy. It is possible that the darkest concentrations do also contain some genuine M 33 stars that cannot be disentangled using the near-infrared colour-magnitude diagram alone. However, these stars are too blue to be AGB stars and their exclusion is appropriate for the analysis presented in this paper. A more detailed investigation of the galaxy structure, combining optical and near-infrared photometry, will be presented elsewhere.

3.3. Subdivision of the M 33 area

To study the spatially resolved SFH, the area occupied by M 33 stars was divided into five elliptical rings and each ring has been divided into eight sectors. Figure 5 shows these regions after converting to polar coordinates using as a reference centre $(\alpha, \delta) = (23.46°, 30.66°)$ (van den Bergh 2000). The position angle of the major axis of each ellipse is 23° (van den Berg 2000). Each ellipse is such that the semi-minor axis $b = a/3.4$ where a is the semi-major axis and corresponds to 0.127°, 0.199°, 0.275°, 0.384° and 0.7° from the inner to outer ellipse respectively. This relation has been obtained from the galaxy parameters listed by NED: $2a = 70.8'$ and $2b = 41.7'$. The size of the semi-major

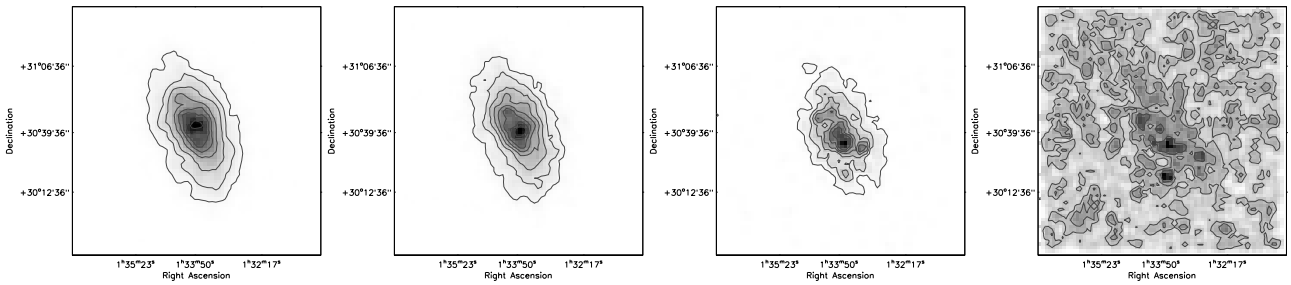

Fig. 4. *(From left to right)* Distribution of the number density of C stars, M stars, super giant stars and mostly foreground stars. See the text for the selection of each sample. Contours are at: 3, 9, 18, 33, 45, 55, 65 and 75 for C stars, 2, 5, 10, 15, 20, 25, 30 and 35 for M stars, 0.5, 2, 4, 6, 8 and 10 for super giant stars, and 1.4, 2 and 3 for foreground stars. Darker regions correspond to higher numbers. North is to the top and East is to the left.

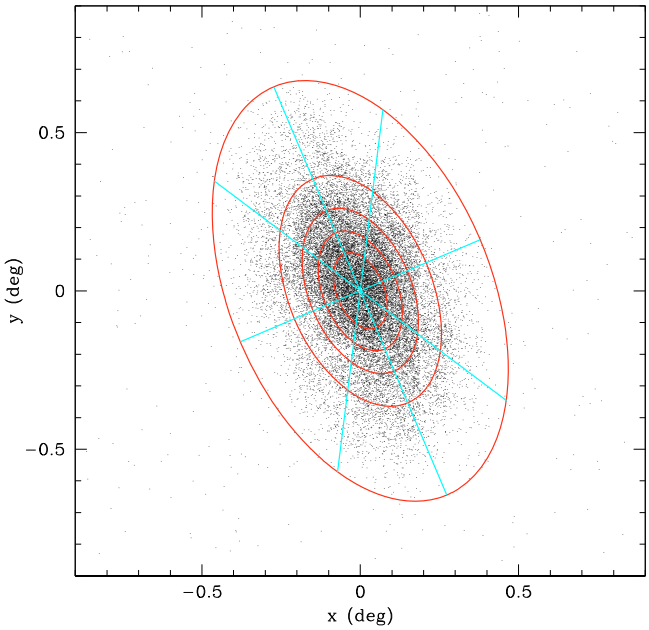

Fig. 5. Distribution of C-rich AGB stars across M 33. Coordinates are in degrees and are centred at $(\alpha, \delta) = (23.46°, 30.66°)$ according to van den Bergh (2000). Sectors of elliptical rings defining the regions used in this study are clearly indicated. Each ring contains an approximately equal number of stars. North is to the top and East to the left.

axis of each ellipse has been determined such as each elliptical ring contains approximately the same number of C-rich AGB stars (≈1470 and ≈1900 using the *vertical-* and the *slanted-lines* selection criteria, respectively). Each ring comprises ∼3500 O-rich candidate AGB stars depending on the selection criteria. These numbers give a statistical significant sample of AGB stars per sector to use for the determination of the mean age and metallicity across the galaxy.

The distribution of C-rich and O-rich AGB stars as a function of $K_{s,0}$ magnitude within each ring are shown in Figs. 7 and 8. Sources selected using both criteria are compared. The shape of the histograms is likely to affect the determination of the SFH parameters more than the overall number of sources, because theoretically produced K_s magnitude distributions are scaled to the absolute number of C-rich AGB stars observed. A separation of C-rich AGB stars at $(J - K_s)_0 = 1.36$ clearly selects less faint stars, but also less stars of mid-range brightness, see in particular the distribution in the outermost ring (Fig. 7). This criterion includes super giant stars in the distribution of O-rich AGB stars as well as faint candidate AGBs which are excluded by the other criterion. However, the shape of the overall distribution of O-rich AGB stars in the different rings is rather similar (Fig. 8).

3.3.1. Completeness and confusion

By selecting stars with an uncertainty in magnitude better than 10% within each ellipse it is possible to evaluate the effect of crowding on the faintest detectable source. In the K_s band the mean magnitude of stars with photometric errors of 0.10 ± 0.01 is 18.15 in the central ellipse, which corresponds to the discontinuity caused by the tip of the RGB, and increases with a step of ∼0.03 mag outwards for each ellipse attaining a value of 18.30 in the outermost ellipse. In the J band it is 18.89 in the central ellipse and 19.17 in the outermost ellipse with a step of ∼0.07 mag. All these values, and especially those in the three innermost ellipses, are well above the expected position of the tip of the RGB in the J band. On the other hand, it is common practice to accept sources with a $S/N = 5$ as good detections. This corresponds to increasing the tolerance to photometric errors as large as ∼0.2 mag. Repeating the same calculation in each ellipse we obtain: $K_s = 18.98$ (inner ellipse) and $K_s = 19.75$ (outer ellipse) as well as $J = 19.12$ and $J = 20.05$, respectively. These values indicate that any AGB star brighter then the tip of the RGB was sufficiently well detected to be included in the following analysis.

However, it remains to be checked how these values compare with the level of confusion. This can be done by extrapolating the cumulative distribution of the extracted sources and calculating the source density within each ellipse. A source density of 1 per 30 beams represents the confusion limit but for very dense fields 1/50 is a better rule (Hogg 2001). Considering that the average seeing of 1.07″ (Sect. 2) is much larger than the instrumental point spread function (0.4″), it is the seeing that defines the beam and the confusion limit corresponds to $50 \times \pi(1.07''/2.35)^2 = 32$ arcsec^2. assuming a gaussian point spread function. This occurs at $K_s = 18.55$ and $J = 18.48$ in the central ellipse suggesting that AGB stars might be confusion limited in the J band. For any other ellipse the magnitudes of AGB stars are well above the confusion limit of one source per 32 arcsec^2.

The number density has been estimated utilising all extracted sources. In particular, most of these are stellar-like or non-stellar objects in roughly equal numbers. The spatial distribution of the latter is mostly confined within the inner ellipses of the galaxy suggesting that many of these sources are the result of

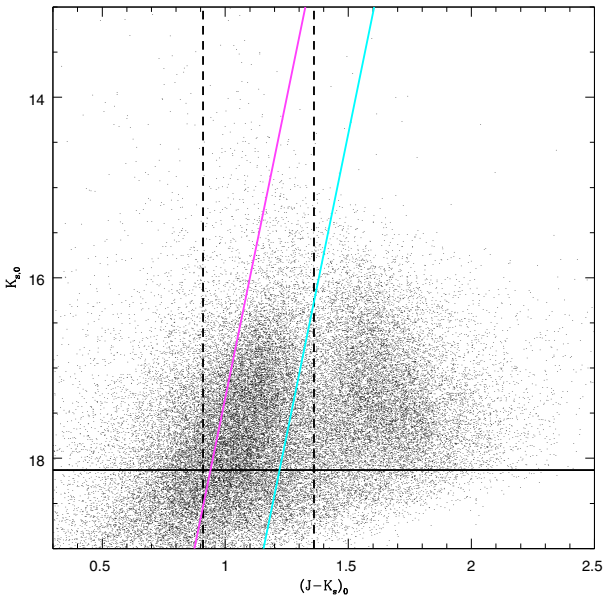

Fig. 6. Colour-magnitude diagram of the non-stellar sources detected in J and K_s across M 33. Many of these sources are blends but there are also HII regions, associations and background galaxies. Lines are like in Fig. 2.

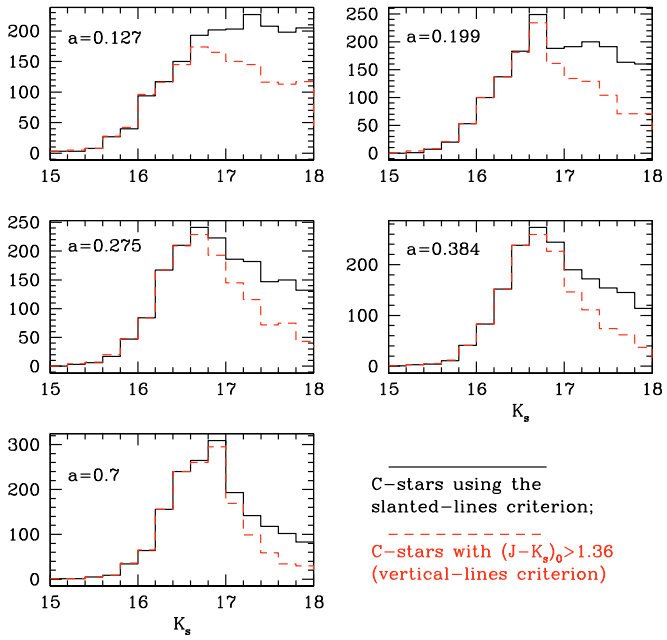

Fig. 7. Distribution of the number of C-rich AGB stars within each elliptical ring. Rings are marked with the value of the semi-major axis (degrees). The selection of sources performed using *slanted lines* is shown by continuous-line histograms while the selection using *vertical lines* is shown by dashed-line histograms. Bins are of 0.2 mag.

merging and crowding instead of genuine HII regions or associations. Others, distributed throughout the field observed, are likely background galaxies. The distribution of non-stellar objects in the ($J - K_s$, K_s) colour-magnitude diagram (Fig. 6) outlines two broad branches: the most populous overlapping the distribution of O-rich giants and the other, almost symmetric, at 0.5 redder colours.

3.3.2. Structure and extinction

In order to interpret the distribution of age and metallicity across M 33 we need to account for its structure and in particular for the parameters that characterise the AGB disc (position angle and inclination). The plane of the galaxy is inclined with respect to the line of sight by $i = 56° \pm 1°$ (Zaritsky et al. 1989). According to van der Marel & Cioni (2001) this would produce a sinusoidal variation of the magnitude of objects with identical properties at a given distance from the centre with position angle (Φ). Based on geometrical considerations the amplitude of this variation can be described as $A = 0.038\rho \tan i$ where $\rho = \sqrt{(x^2 + y^2)}$ is the angular distance from the centre expressed in degrees. AGB stars in M 33 can be traced to a maximum distance of 0.7° which corresponds to detecting a maximum amplitude of 0.04 mag.

The presence of differential extinction may also significantly alter the determination of the mean metallicity and age using the K_s magnitude distribution of AGB stars. In order to evaluate the effect of differential extinction across M 33 we need to study the variation of features tracing extinction across the galaxy. In the near-infrared the colour $J - K_s$ as well as the mode of the distribution of individual magnitudes represent these features. Note that any, albeit small, variation due to the orientation of the galaxy in the sky (see above) will also be included. In particular, magnitudes are degenerate in both parameters (structure and extinction) while colours better represent reddening.

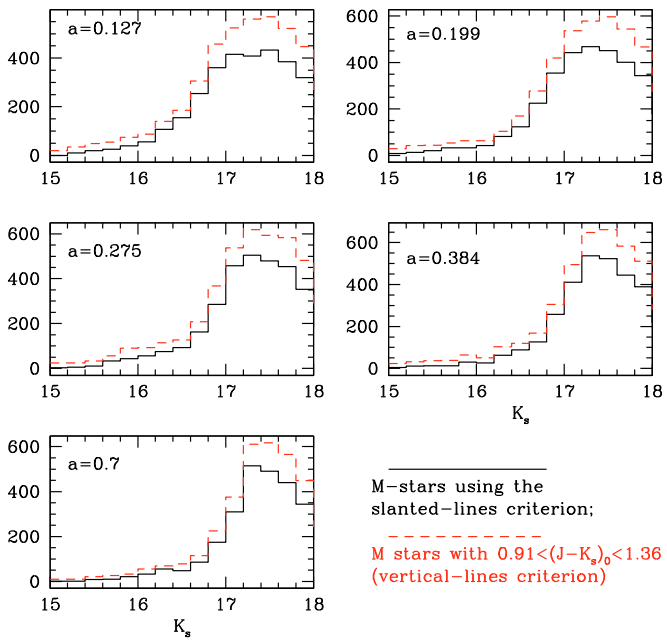

Fig. 8. The same as for Fig. 7 but for O-rich AGB stars.

By subdiving the M 33 area into the same eight sectors as shown in Sect. 3.2 three elliptical ring areas were defined. Their outer semi-major axis corresponds to 0.2°, 0.4° and 0.7°, respectively, and comprises a sufficiently large statistical number of AGB stars to measure the effect of orienation and extinction. Histograms of the number of AGB stars versus each near-infrared magnitude and $J - K_s$ colour were constructed adopting a bin size of 0.1 in mag and 0.05 in colour within each

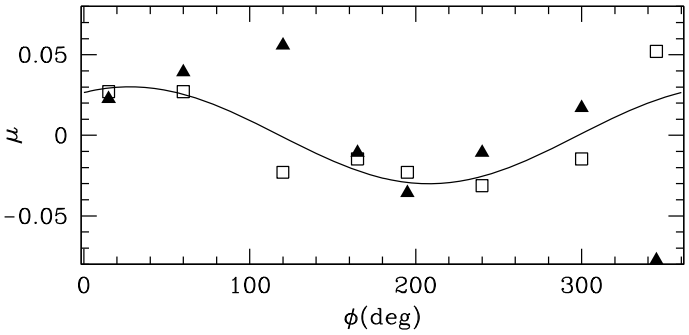

Fig. 9. Distribution of the difference between the peak of magnitudes (squares) and colours (triangles) of C stars within 8 sectors and their average of a unique ellipse with a semi-major axis of 0.7° versus PA (see text for details). The best fit sinusoid has a half amplitude of 0.03 ± 0.01 mag and corresponds to $\phi = 28° \pm 6°$. This angle is measured on the plane of the galaxy where 0° corresponds to the NE point of the major axis and increasing to the East. Errors on each point are at most 0.02 mag and have been omitted for clarity.

elliptical ring. In particular, C and M stars, brighter than the tip of the RGB, were selected within narrow ranges of colours: $1.5 < (J - K_s)_0 < 2.0$ and $1.0 < (J - K_s)_0 < 1.3$, respectively, to avoid contamination from one spectral type to the other. The bin defining the mode of each histogram contained 20−30 stars each with a photometric error of ≤0.1 in magnitude and ≤0.25 in colour which correspond to an uncertainty of at most 0.02 mag in the determination of the peak position.

The average distribution of the peak position of magnitudes and colours of C stars for all ellipses traces a well defined sinusoid with a half amplitude of 0.03 ± 0.01 mag and a position angle $\phi = 28° \pm 6°$ (measured on the galaxy disc where 0° corresponds to the NE point of the major axis and increasing to the East) with $\chi^2 = 0.001$ (Fig. 9). Each point in this figure corresponds to equal sectorial areas of a single ellipse with semi-major axis of 0.7°. In the usual astronomical convention where sky angles are measured from the North increasing to the East this is equivalent to $\Phi = 51° \pm 6°$. Despite the moderately small error associated to the position angle, the sinusoid has a rather flat maximum as well as minimum which suggest a larger uncertainty in the accuracy of these features. M stars are consistent with a similar pattern but present a larger scatter resulting in a larger χ^2 while a variation in the bin size has a small effect on these numbers.

It is, however, surprising that both magnitudes and colours describe a very similar sinusoidal pattern. If all near-infrared magnitudes would strictly describe the same variation then the variation in the colours should be close to zero. By inspecting the variation in the J, H and K_s bands separately we conclude that while H and K_s behave similarly, and produce a best fit sinusoid with $\phi = 353°$ and amplitude 0.04 mag, the variation in the J band is at odds ($\phi = 80°$ and amplitude 0.04 mag). This has two effects: decreasing the amplitude of a sinusoid that aims to fit all three near-infrared magnitude variations and inducing a sinusoidal variation in the $J - K_s$ colour (Fig. 9). If the detected variation in colour would only be due to extinction the magnitude variation could be corrected accordingly. Interstellar absorption in a given wave band is usually stronger at J than at K_s, this might explain why the variation in J disagrees with the variation in the other redder wave bands. Because this study focuses on the K_s magnitude we have used the average sinusoid shown in Fig. 9 to correct for structural and reddening effects. This is a conservative approach in view of the uncertainties in the previous considerations.

The mean magnitude within each ellipse varies as a function of radius increasing by about 0.08 mag from the inner to the next outer ellipse. This variation is much larger than the variation derived above attributed to the orientation and extinction of the galaxy and suggests a non-negligible variation in the age and/or metallicity of the stellar population. These variations are usually of radial type. The size of the three ellipses considered in this study is such that the middle one corresponds to the metal-poor ring-like structure suggested from the distribution of the C/M ratio (Fig. 10).

Dust in the M 33 disc might follow a patchy rather than regular distribution, as assumed above. If the size of a dusty patch is comparable to the size of one or a few bins, thus much smaller than individual sectorial regions used to build histograms, then the method adopted in this paper does not account for it. A detailed reddening map that will allow us to correct the photometry of each source prior the construction of histograms of their distribution is not yet available.

3.4. Distribution of the C/M ratio

The ratio between C-type and M-type stars is a simple indicator of metallicity. A high number of C stars, and therefore a high C/M ratio, is typical of metal-poor environments. Stars are of C-type when their atmosphere contains more carbon than oxygen atoms apart from those that are coupled into CO molecules. C atoms are dredged-up from the stellar interior to the atmosphere during stellar evolution. If the metal content at the time when stars formed was low it is easier to form C-stars than vice-versa. The correlation between the C/M ratio and [Fe/H] has been empirically determined and was recently calibrated by Battinelli & Demers (2005). Cioni & Habing (2003) have used this ratio to clearly show the presence of a metallicity gradient within the Large Magellanic Cloud (LMC). However, this ratio depends on the age of the underlying stellar population as was shown by Cioni et al. (2006a). The age parameter is further discussed in Sect. 3.5.

The surface distribution of the C/M ratio across M 33 is shown in Fig. 10. The top panel shows the distribution obtained selecting stars using the *slanted-lines* criterion while the bottom panel shows the distribution obtained using the *vertical-lines* criterion. Both distributions have been obtained applying a box car smoothing to the ratio calculated using bins of 1.2′. Grey-scaled distributions appear remarkably similar: the outermost parts of the galaxy show a low ratio most probably affected by a low number statistics, immediately inwards dark regions of a high ratio are distributed in a ring-like structure surrounding an inner region with a low ratio but also rather patchy. Maps with twice a lower resolution emphasise the ring-like distribution traced by regions of a high ratio compared to the inner part of the galaxy (Fig. 11). However, using larger bins obviously smoothes fine details inducing the NW region of enhanced ratios to become more prominent than the corresponding SE region. According to Battinelli & Demers (2005) the range spanned by the C/M ratio in Fig. 10 corresponds to a spread in [Fe/H] of at least 0.6 dex. In particular, the most metal-poor regions of the galaxy have [Fe/H] = −1.54 dex while the most metal rich have [Fe/H] = −0.91 dex.

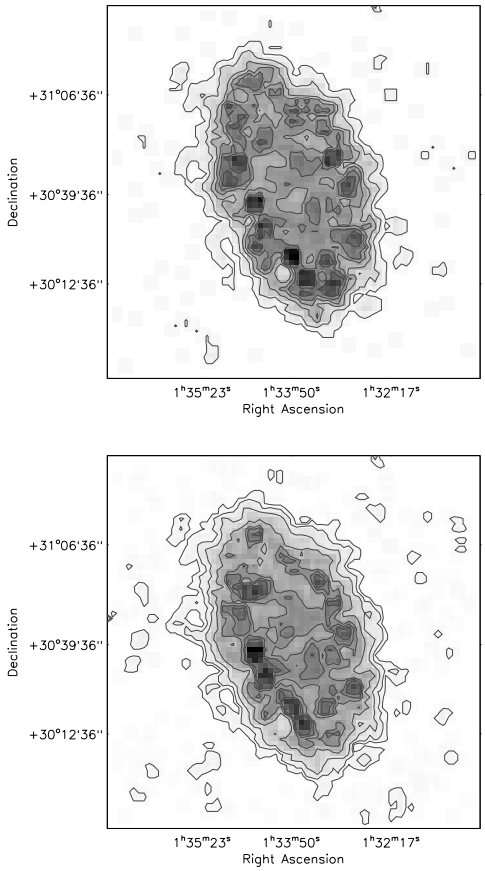

Fig. 10. Distribution of the C/M ratio across M33. C-rich and O-rich AGB stars above the tip of the RGB have been selected using slanted lines (*top*) or using vertical lines (*bottom*). Darker regions correspond to higher ratios. Contours are at: 0.2, 0.6, 1.2, 1.6, 2.0 and 2.4 in the *top panel* and at 0.25, 0.5, 1.0, 2.0, 3.0, 3.5 and 4.0 in the *bottom panel*.

3.5. Determination of metallicity and mean age

The distribution of AGB stars as a function of K_s magnitude in each sector have been compared with theoretical distributions as in Cioni et al. (2006a) where a detailed description of the stellar evolutionary models adopted is also given. Briefly:

- JK_s-band photometry has been simulated using the TRILEGAL population synthesis code (Girardi et al. 2005), that randomly generates a population of stars following a given SFR, age-metallicity relation and initial mass function;
- bolometric magnitudes, used to derive K_s magnitudes, were obtained by applying the extended tables of bolometric corrections (BCs) from Girardi et al. (2002) for O-rich stars and by empirical relations for C-rich stars: the BC in the K band is taken from the relation by Costa & Frogel (1996) and the $(J-K)$ colour is derived from the $T_{\rm eff}-(J-K)$–C/O relation from Marigo et al. (2003), which itself is based on to the empirical data by Bergeat et al. (2001);
- the stellar properties are interpolated over a large grid of stellar evolutionary tracks, based on Bertelli et al. (1994) and Girardi et al. (2003) for massive stars, Girardi et al. (2000) for low- and intermediate-mass stars and complemented with grids of thermally pulsing AGB tracks calculated by means of Marigo et al.'s (1999, 2003) synthetic code. We refer the reader to the paper published very recently by Marigo et al. (2008) where details about different stellar isochrones, released at different moments in time, are discussed and new computations presented. The main difference between the isochrones adopted in this study and those just released is in the inclusion of the treatment of dust in the thermally pulsing AGB phase. This affects more AGB stars with thick circumstellar envelopes, which have $J-K_s>2$, than AGB stars with thin circumstellar envelopes which represent the bulk of the AGB population analysed in this study of M 33. In particular, Marigo et al. (2008) show that very few O-rich AGB stars, with high mass-loss rates, occupy the region of $(J-K_s)$ colours where most C-rich AGB stars are located. Note also that the M 33 data are photometrically calibrated using 2MASS which is suitable for comparison with the Cioni et al. (2006a) isochrones.

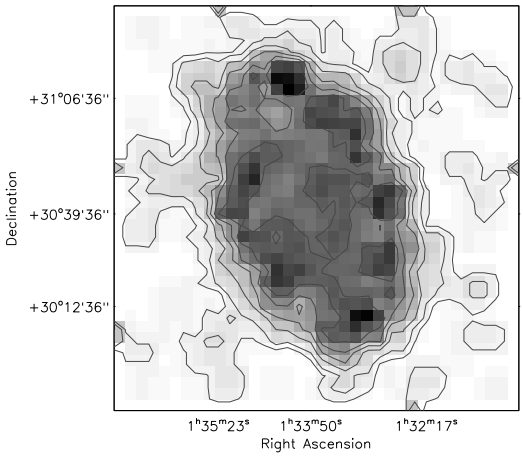

Fig. 11. The same as the *bottom panel* of Fig. 10 but using bins of 2.4′. Contours are at: 0.25, 0.5, 1.0, 1.5, 2.0 and 2.5.

Theoretical distributions were created for 5 different metallicities ($Z=0.0005, 0.001, 0.004, 0.008$ and 0.016) and for 5 different star formation rates (SFRs). The latter adopts a simple family of exponentially increasing/decreasing SFRs, $\psi(t)\propto\exp(t/\alpha)$, where t is the stellar age in Gyr, and α is a free parameter that was taken to have values of: -5, -2, 2 and 5; the special case of a SFR constant in time corresponds to $\alpha=1000$. The mean age of all stars formed in a model with a given value of α is given in Table 1 of Cioni et al. (2006a). The youngest population explored corresponds to a mean age of 2 Gyr and the oldest one to 10.6 Gyr. The step in mean age between adjacent models is at least 2 Gyr. Models were constructed at the distance of the LMC ($(m-M)_0=18.4$) and have been shifted by 5.9 mag to fit the population of M 33. Both *vertical-* and *slanted-lines* criteria to distinguish M-type from C-type AGB stars have been applied to the simulated colour-magnitude diagrams and were adjusted accordingly by the metallicity effect on the $(J-K_s)$ colour (see Cioni et al. 2006a, for details). Note that, similarly to Cioni et al. (2006a), only the K_s magnitude distribution of AGB stars is used. This is the wavelength that best approximates the bolometric luminosity of AGB stars (with thin circumstellar envelopes), in particular carbon stars for which these theoretical models are well calibrated (i.e. using the C stars luminosity function of Magellanic Cloud clusters; Marigo et al. 1999). Before comparing observed with theoretical distributions we corrected for the sinusoidal pattern derived in Sect. 3.3.2. This variation represents an average effect between extinction and orientation of the AGB disc. In practice, K_s histograms have been shifted by

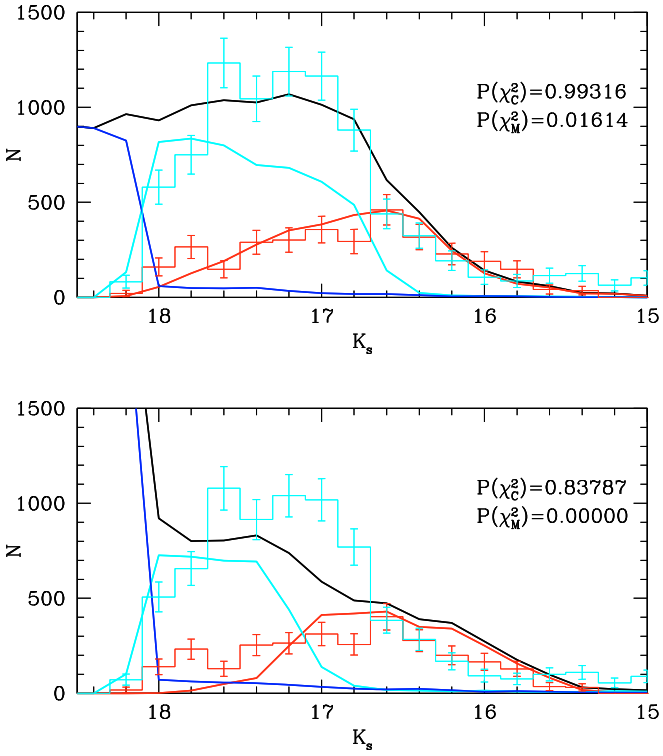

Fig. 12. Comparison between the observed K_s magnitude distribution of C and M stars (histograms) and theoretical distributions. The probability that a given model represents the observed distributions, associated to the χ^2 value, is indicated. These histograms are fitted with models corresponding to a SFR with $\alpha = 5$ (or a mean age of 8.7 Gyr) and a metallicity $Z = 0.0005$ (*top panel*) or $Z = 0.001$ (*bottom panel*). In the electronic version of this figure C stars are in red, M stars in light blue, the sum of C and M stars is in black while RGB stars are in dark blue.

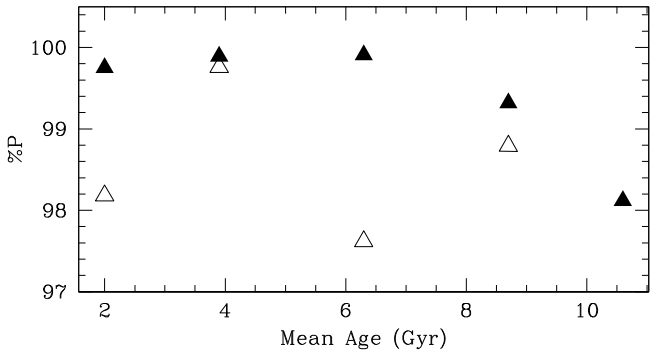

Fig. 13. Probability as a function of mean age for models of a given metallicity which represent the stellar population of M 33 in a sector of a ring. Different symbols refer to a different metallicity as follows: $Z = 0.0005$ (filled triangles), $Z = 0.001$ (empty triangles). Other models explored in this study give a probability much lower than the values plotted here and are not shown.

0.001−0.029 mag depending on their mean ϕ coordinates, regardless of their distance from the centre, in a direction (+/−) that compensates for the sinusoidal variation shown in Fig. 9.

Figure 12 shows examples of the fit of the observed distributions of C and M stars with theoretical distributions obtained from a given model. In this case the observed number counts refer to a sector of a ring while models corresponds to a SFR with $\alpha = 5$ (or a mean age of 8.7 Gyr) and metallicity $Z = 0.0005$ or $Z = 0.001$. In the top panel the interpretation of C stars is good at the 99% level and it reduces to 84% for an increasing metallicity, for M stars it is rather poor in both cases (0−1%). The probability of fitting the same observed distribution of C stars with the whole range of model distributions examined in this study is shown in Fig. 13. The point corresponding to the highest probability indicates that the overall population, within this sector, is metal poor ($Z = 0.0005$) and with a mean age of ∼6 Gyr. This figure also shows the level of uncertainty associated to the metallicity and age quantities. For example: $Z = 0.0005$ gives systematically better fits at any age while the difference between a 2, 4 or 6 Gyr mean age does not seem sufficiently strong. Note that this is just an example for one sector of one ring, and the uniqueness of a model fit across the whole galaxy can therefore be estimated from the probability maps (Fig. 14). The similarity of some of the maps shown suggests that the difference in age is not robustly determined or on the contrary that there is a large spread in mean age.

The distribution of metallicity separately for different SFRs and the probability that a given model represents the observed distribution of C stars, selected with both criteria, are shown in Fig. 14. In order to create each of the maps shown, first, we made a grid of 13 395 points with coordinates $-0.47° \leq x \leq 0.47°$ and $-0.7° \leq y \leq 0.7°$, in the plane of the galaxy, equally spaced with a step of 0.01°. Then, we assigned to each point the quantity (age, metallicity and likelihood – the probability of getting a χ^2 value) accordingly to which sector a point belongs. We rebinned the distribution of values in bins equal to 0.04° (this corresponds to a resolution of 2.4′), smoothed the intensity with a 2×2 box car function and restored the orientation of the galaxy in the sky. Finally, we constructed greyscale maps where darker regions correspond to higher numbers. Similar maps were created also for the distribution of O-rich AGB stars, however, these individual maps are not shown here while Figs. 15 and 16 show combined maps for both AGB spectral types. These maps were obtained by choosing the theoretical distributions of AGB stars that correspond to the smallest χ^2 value among those generated from each combination of SFR and metallicity, for a given sector of a given ring. Note that due to the approximations involved in building-up the theoretical distribution absolute values of mean age and metallicity should be taken with care. Much more important are their variations across the galaxy.

3.5.1. Distribution of metallicity versus mean-age

The maps resulting from almost all different cases of SFR and AGB selection criteria shown in Fig. 14 suggest that the metallicity in the centre of the galaxy is different from the metallicity in the outer regions. In particular, the best metallicity that fits the overall disc of M 33 is the lowest explored in this study which suggests a stellar population metal poorer than $Z = 0.0005$ or at least as metal poor as $[M/H] = -1.6$ dex assuming $Z_\odot = 0.02$ (Figs. 14, 15) and using the conversion $[M/H] = \log(Z/Z_\odot)$ where $[Fe/H] \leq [M/H]$. Approaching the centre of the galaxy there are well defined and relatively small regions rich in metals ($[M/H] = -1.2$ dex). These regions change location depending on the SFR and AGB selection criterion considered. The time sequence shown in the top row of Fig. 14 shows that both for a very old and a very young age a metal-rich nucleus is present and it is slightly displaced from the centre of the galaxy. However, this is the region where the data are the least reliable as shown from

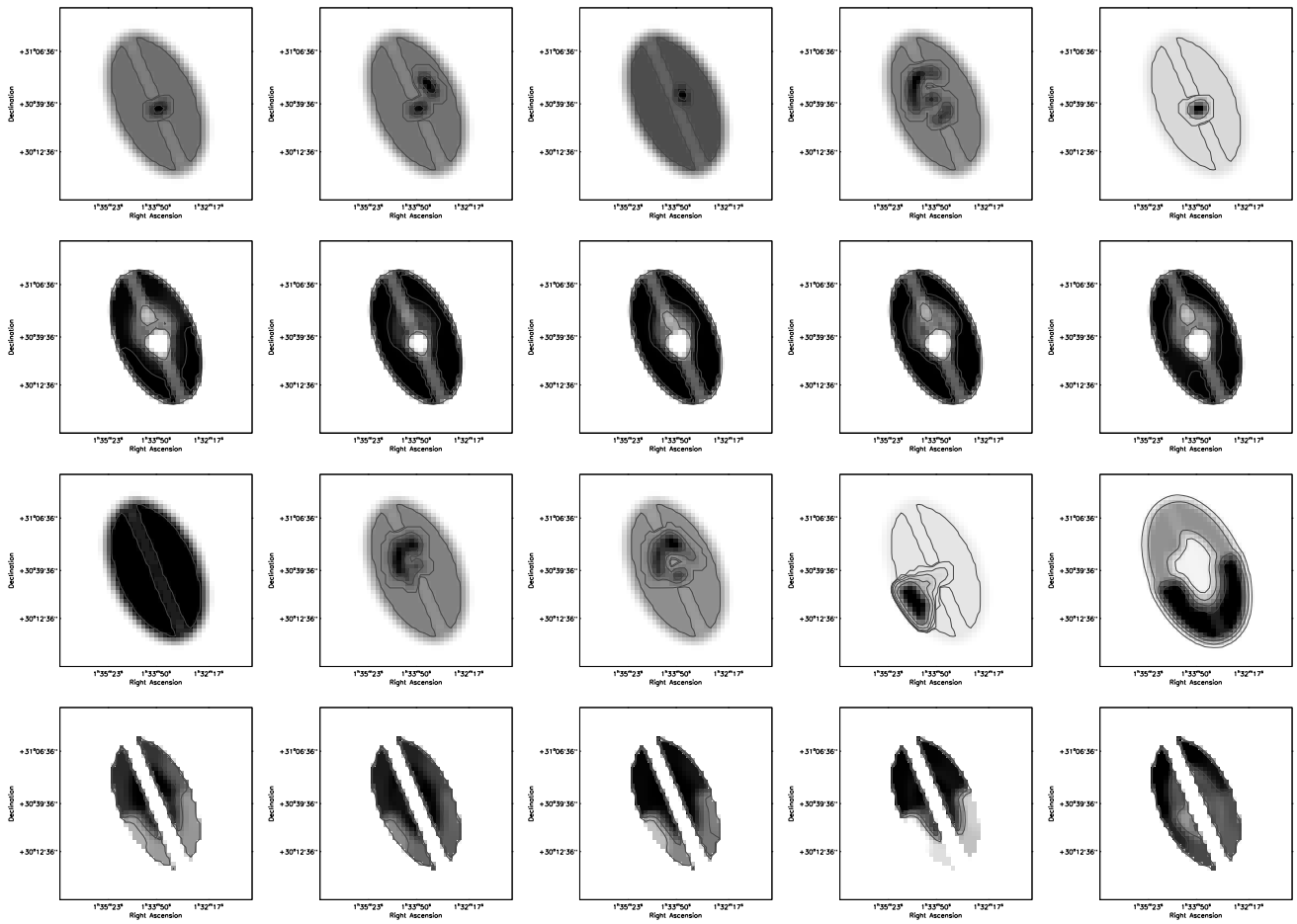

Fig. 14. Surface distribution of the most probable metallicity (*first and third rows)* at a given SFR (or mean age) and the associated probability distribution (*second and fourth rows*) obtained by fitting the K_s magnitude distribution of C stars. C stars have been selected from the near-infrared colour-magnitude diagram (Fig. 2) using vertical lines (*top two rows*) and using slanted lines (*bottom two rows*). *From left to right each column* refers to a mean age of 2, 3.9, 6.3, 8.7 and 10.6 Gyr, respectively. Contours for each panel in the *top row* are at $Z = 0.00048$ (panel 1); 0.00048, 0.0005, 0.0006 and 0.0007 (panels 2 and 3); 0.00048, 0.0005, 0.0006, 0.0008, 0.0012 and 0.002 (panel 4); 0.001, 0.003, 0.005 and 0.007 (panel 5). Contours for each panel in the *third row* are at $Z = 0.00048$, 0.0005, 0.0006 and 0.0007 (panels 1, 2, 3, 4); 0.00048, 0.0005 and 0.001 (panel 5). The grey scale for the probability distributions shows only values above 0.7 (contours are at 0.85, 0.95 and 0.99) and 0.95 (contours are at 0.97, 0.98 and 0.99) for the *second* and *fourth* rows respectively. Darker regions correspond to higher values.

the probability maps. At other intermediage ages an additional metal-rich clump is located NW of the nucleus. The metal-rich spiral pattern corresponding to a mean age of 8.7 Gyr does not have to be associated with the NW bump. It is popular to speculate that a structure has been accreted by M 33 in the past and is now well mixed with the disc population. The variation of mean metallicity perhaps suggests the propagation of the star formation with time. The comparison with maps shown in the third row of Fig. 14 should guide the reader on the differences due to the different way AGB stars can be selected from the near-infrared CMD. Here, the metal-poor disc is also recovered while the metal-rich internal structure describes a broken ring in the Northern part of the galaxy, a minor clump in the centre and for the oldest ages a wide metal-rich area encompassing the outer Southern region of the galaxy prior to a clump enriching in metals from the centre to the SE. The probability that the latter is a real effect is not very high as well as for the values recovered in a stripe across the major axis of the galaxy. There is currently no explanation on why the major axis appears as a critical region in most of the maps.

3.5.2. Combined distributions of mean-age and metallicity across M 33

Figure 15 shows the combination of the individual maps of Fig. 14 corresponding to the lowest χ^2 for each sector of each ring and pair of metallicity and SFR parameters. Taking the values that correspond to the highest probability (lowest χ^2) represent a first order approximation to the average parameters of the stellar population at a given location within the galaxy. In some cases, e.g. Fig. 13, a combination of those values with high probabilities may be more appropriate. Contrary to individual maps, combined maps do not show a region of low statistical significance around the galaxy major axis. This is because at each point in the map the most reliable metallicity is chosen and grayscales and countours are adapted accordingly. The lowest contour of the metallicity distribution for both selection criteria confirms a disc population metal poorer than [M/H] = −1.6 dex. Regions with an associated higher metallicity are often those which are less reliable (have larger values of χ^2); the reliability is higher if C stars are selected using the *vertical line* criterion. The nucleus,

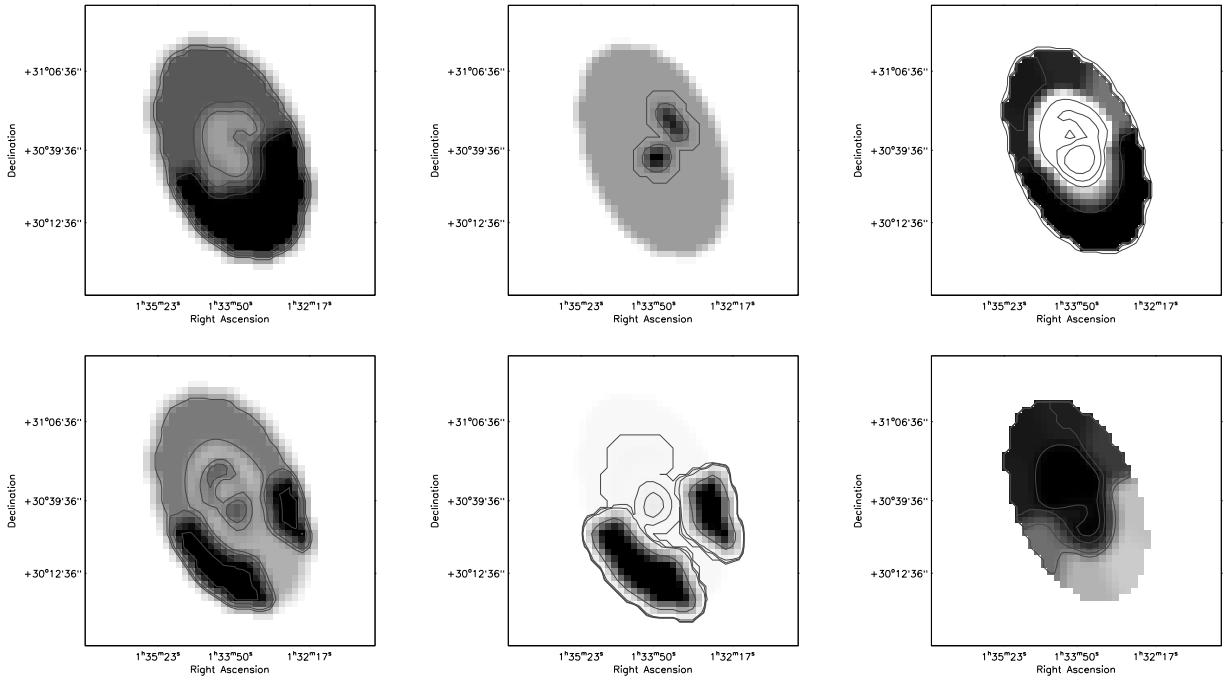

Fig. 15. Spatial distributions of the mean age of the stellar population of M 33 (*left*), of the metallicity (*middle*) and of the statistical probability that expresses the confidence level of the previous distribution. These distributions have been constructed from the comparison between the observed K_s magnitude distribution of C-type AGB stars with theoretical distributions. C stars have been selected from the colour-magnitude diagram (Fig. 2) using vertical lines (*top row*) or slanted lines (*bottom row*). Bins are of 2.4′ and dark regions correspond to high numbers. *From left to right* contours are at: 5, 6, 7, 8 (*top*) and 5.5, 6.5, 8.5, 10.5 (*bottom*) Gyr for age; 0.0005, 0.0006 (*top*) and 0.0005, 0.0006, 0.0008, 0.004 (*bottom*) for metallicity where only values above 0.0002 are displayed; 0.992, 0.994, 0.996, 0.998, 0.999 where only values above 0.98 are displayed (*top*) and 0.85, 0.95, 0.98, 0.999 where only values above 0.98 are displayed (*bottom*) for probability.

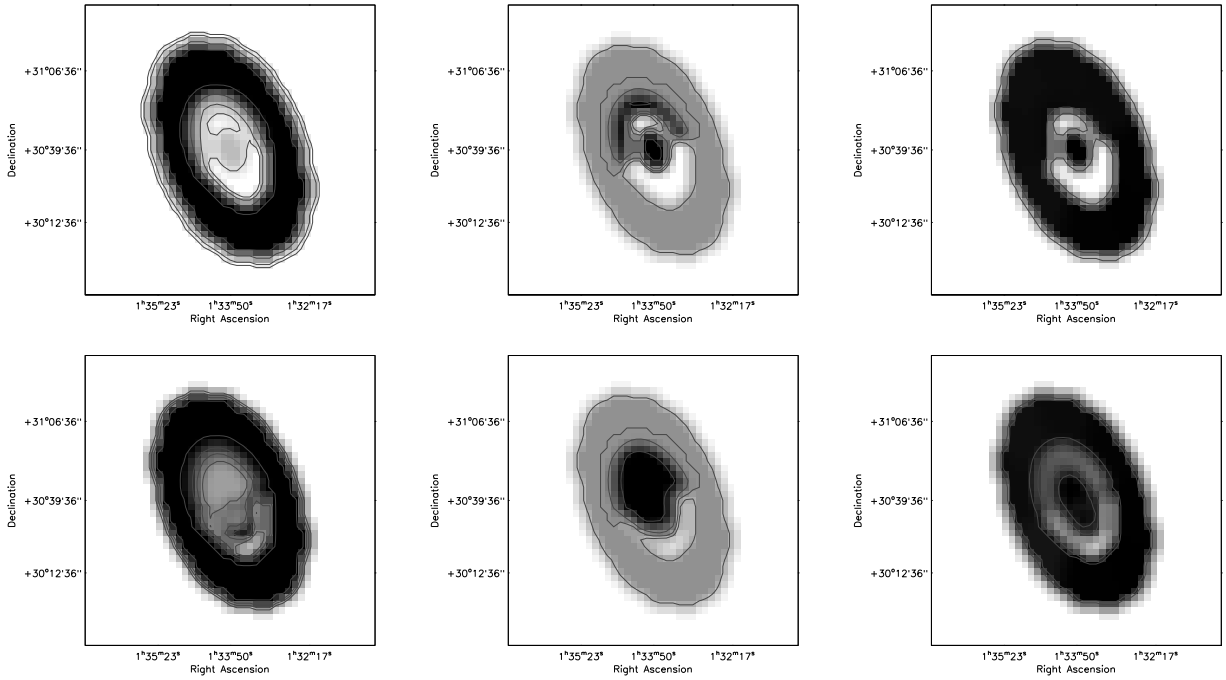

Fig. 16. Spatial distributions of the mean age of the stellar population of M 33 (*left*), of the metallicity (*middle*) and of the statistical probability that expresses the confidence level of the previous distributions (*right*). These maps have been constructed from the comparison between the observed K_s magnitude distribution of M-type AGB stars with theoretical distributions. M stars have been selected from the colour-magnitude diagram (Fig. 2) using vertical lines (*top row*) or slanted lines (*bottom row*). Bins are of 2.4′ and dark regions correspond to high numbers. *From left to right* contours are at: 1, 2, 4, 6 (*top*) and 5, 6, 7, 8.5 (*bottom*) for age; 0.0065, 0.008, 0.01, 0.015 (*top and bottom*) for metallicity; 0.5, 0.8 (*top*) and 0.8, 0.9 (*bottom*) for probability.

as seen before, is as metal rich as [M/H] = −1.2 dex as well as a region NW of it.

The distribution of mean age is quite similar between both selection criteria. It shows a broad outer ring which is older (∼6 Gyr) than the region within it, except perhaps for the nuclear region. If C stars are selected using the *slanted-lines* criterion both the centre and a small region NE of it are as metal rich as the outer ring. On the other hand, if the other criterion is used then the broad old ring is slightly wider while the centre is the metal poorest. It also appears that the Southern parts of the outer ring are older than the Northern parts of it. This apparent asymmetry might be a residual from the correction for the orientation and extinction within the galaxy (Sect. 3.3.2). We have taken a conservative approach of averaging the variation obtained from colours and magnitudes across the galaxy. If only the azimutal variation in the K_s band were considered then stars in the North would be fainter than stars in the South – the peak of the sinusoidal variation would be at 0° for an amplitude up to 0.05 mag (slightly larger than the one adopted in the correction). These new parameters, however, would also affect the distribution of metallicity, this might be true for the *slated-lines* criterion but it is not the case for the other criterion. It is possible that including fainter and bluer C-rich stars that might be instead O-rich reveals a N-S asymmetry. This feature has therefore a low statistical significance.

Overall the significance level of both the distribution of mean age and metallicity across the surface of the galaxy is high (>98%) which indicates that there is a theoretical model (a combination of metallicity and SFR) that describes the observed K_s-band distribution rather well. Simply by comparing the probability distributions obtained from the two selection criteria adopted it is evident that selecting C stars using *vertical lines* produces a sample that is better fit by theoretical distributions across the galaxy (see also Fig. 14). This criterion is perhaps conservative because it excludes faint AGB stars, known to exist in mixed stellar populations, but it does show the distribution of the bulk of the C star population of this galaxy. Therefore we regard the top row of Fig. 15 as trustworthy in the interpretation of age and metallicity variations across M 33 as derived from C stars.

Similar maps derived from the distribution of M-type stars are shown in Fig. 16. The most reliable results are obtained for the outer ring and for the centre. It is well confirmed that the outer ring is old (6−8.5 Gyr depending on selection criteria) and metal poor although the latter corresponds to a much higher metallicity than that derived from C stars. These maps suggest that the centre of the galaxy is metal rich and younger which is also in agreement with the pattern obtained from C stars. It is also possible that North of the centre another broken ring-like structure supports a higher metallicity while in the South the same structure will be metal poor. The latter is the least constrained result. Note that the fit of the sample of M stars obtained using the *slanted-lines* criterion corresponds to a higher probability than the fit obtained from a sample selected using the *vertical-lines* criterion. Figure 2 shows that the latter isolates the bulk of the M star population of M 33, this is perhaps the reason why, despite the current uncertainties on the theoretical representation of M stars, the fits are more reliable although the sample is not complete. The significance level of both the distribution of mean age and metallicity is below the level obtained from C stars. This was also the case in Cioni et al. (2006a) for a similar study of the Magellanic Clouds. It is possible that the models fail to interpret correctly the distribution of M stars or that the model parameters were not sufficiently explored. Very recently Marigo et al. (2007) show that improving the lifetime of M-type stars alleviates the problem of underestimating the stellar populations. In the subsequent discussion more emphasis is placed on C stars.

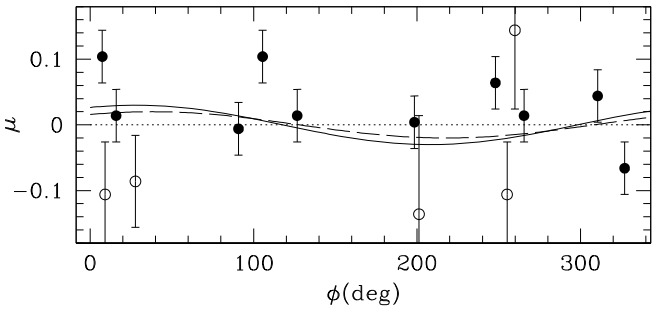

Fig. 17. Distribution of the difference between the individual distance moduli derived by Kim et al. (2002; *filled circles*) and other authors (see text; *empty circles*) and their mean versus position angle. Note that the point corresponding to McConnachie (2005) measurement is outside the range shown of this figure. The *continuous* sinusoid is the same as in Fig. 9 while the *dashed* sinusoid is the best fit to Kim et al. (2002) data only; the zero line is also indicated (*dotted*). Error bars correspond to the random error for Kim et al. (2002) measurements, sytematic errors amount to +0.15 and−0.11, and the global error quoted by the authors for the other points.

Summarizing, the most reliable interpretation of the K_s magnitude distribution of C and M stars is obtained by selecting reliable, whilst not complete, sample of stars using the *vertical-lines* criterion for C stars and the *slated-lines* criterion for M stars. A complete sample can only be obtained via spectroscopic observations of the entire AGB population of M 33 (see Groenewegen 2004, for the Magellanic Clouds).

4. Discussion

4.1. Distance to M 33

Several authors have measured the distance to the M 33 galaxy using different stellar indicators. In particular, Bonanos et al. (2006) obtains a distance modulus of 24.92 ± 0.12 to a detached elipsing binary, Sarajedini et al. (2006) obtains 24.67 ± 0.08 using RR Lyrae stars located in two fields NW and SE of the galaxy centre. Using the tip of the RGB method: Galletti et al. (2004) obtains 24.64 ± 0.15 in a field in the outskirts of the galaxy, Tiede et al. (2004) obtains 24.69 ± 0.07 in a different halo field while Kim et al. (2002) obtains 24.81 ± 0.04 from the average of 10 independent fields distributed throughout the galaxy, mostly in the outer halo but two in the centre. The latter also provide individual measurements for each of these fields. There are many other measurements that have not been cited here and this is because they were obtained from indicators distributed througout the galaxy and provided only one measure of the distance to the galaxy without investigating its variation across it. The point here is not to derive a new distance to M 33 but to show that inconsistencies among previous measurements may be explained by accounting for the orientation and extinction of the galaxy disc.

In Sect. 3.3.2 we showed that magnitude and colour vary according to a well defined sinusoidal pattern which can be attributed to the geometry of the galaxy as well as to the presence of differential extinction. Here, we compare this pattern with the spatial variation of different measures of the distance to the galaxy. Figure 17 shows the distribution of the difference

between each distance measurement and their mean as a function of position angle regardless of their distance from the centre. Error bars correspond to the value estimated for the final distance moduli. In the case of Kim et al. (2002) it is obtained from averaging the ten measurements, and is shown here just as a guideline. The real error bar of each individual point is smaller than the one indicated. The sinusoid derived earlier is overplotted and shows a good agreement, especially with the measurements by Kim et al. (2002), which were homogeneously analysed. This suggests that a sinusoidal variation is likely although current differences from the zero line are not pronounced. Note that we did not correct for the different extinction values used by the different authors and this is partly responsible for the scatter of the distances obtained.

McConnachie's (2005) measurement of the tip of the RGB in the I band differs by 0.13 magnitudes from the measurement of Tiede et al. (2004), both authors studied fields at the same distance from the centre but at diametrically opposite directions. According to our study a variation of 0.06 mag is expected between fields opposite to the centre. Considering that Brooks et al. (2004) by observing an area very similar to that of Tiede et al. (2004) derived a tip of the RGB 0.05 mag fainter as well as other uncertainties in the location of the tip of the RGB, the sinusoidal pattern derived in this study explains the Tiede-McConnachie difference between their tip of the RGB measurements. On the other hand, McConnachie (2005) explains the variation in the measured values of the tip of the RGB as due to differential reddening within the M 33 disc.

What is the main cause of the sinusoidal pattern? If this difference were entirely due to differential extinction a value as large as $E(B-V) = 0.17$ would be obtained assuming $A_{K_s} = 0.06$ and using the Glass et al. (2003) extinction law. It is more likely that at infrared wavelength the extinction plays a small role. On the contrary, an effect due to the orientation of the galaxy would affect each magnitude equally. Therefore, the sinusoidal pattern derived in this study despite including a variation of the stellar population as well as of extinction is predominantly caused by the geometry of the galaxy.

In a rotationally supported spiral galaxy of known geometry, like M 33, the near side is the West side. In Sect. 3.3.2 the sinusoid traced by AGB stars has a rather flat minimum and maximum which suggests a large uncertainty in the determination of the far versus near side of the disc. Moreover, the disc of M 33 is warped. Corbelli & Schneider (1997) have modeled the HI gas distribution across the galaxy. In their study it is clear that the SW and the NE regions are peculiar because this is where the warp sets in, i.e. they mark the beginning of the deviation from the inner (more flat) parts. It is possible that hte analysis of the AGB distribution is affected by the presence of the warp but this suggestion needs to be confirmed.

4.2. Confirmed long-period variables

In this section we compare the distribution of candidate AGB stars selected using the colour-magnitude criteria of Sect. 3.1 with the distribution of confirmed Long-Period Variables (LPVs) from the catalogue by Hartman et al. (2006). We cross-identified our catalogue of near-infrared sources with the LPVs candidates located in a specific region of the $(r - i')$ versus i' colour-magnitude diagram (Hartman et al. 2006, their Fig. 7). We found that 7650 candidates have a near-infrared counterpart within 1″. The histogram of the distance between near-infrared and LPV matches has a narrow peak at 0.15″ with a $FWHM = 0.25''$; these values were obtained after correcting

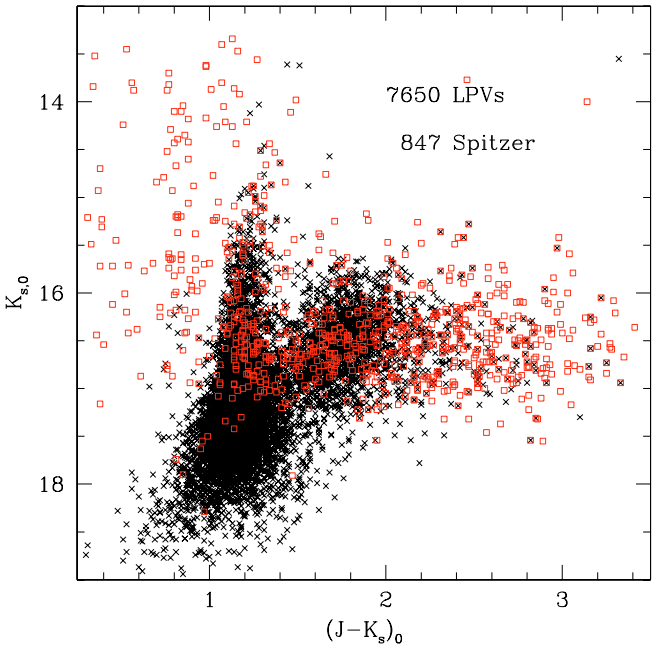

Fig. 18. Colour-magnitude diagram of the near-infrared sources matched with the LPVs (crosses) from Hartman et al. (2006) and the variable stars detected by Spitzer (squares) from McQuinn et al. (2007). A colour version of this figure is available in the electronic version of the paper.

the Hartman et al. (2006) coordinates by a systematic shift in right ascension of 0.4″ (the shift in declination is negligible and amounts to ∼0.05″). The distribution of these sources is shown in Fig. 18. The branch of C-rich AGB stars departing to red colours as well as the vertical branch of O-rich AGB stars are clearly distinct supporting the selection criteria presented in Sect. 3.1. The table with the near-infrared photometry from our study and the optical photometry by Harman et al. (2006), of which an extract is given in Table 1, is available electronically; coordinates are from UKIRT data.

Block et al. (2004) claim to have observed the brightest unresolved C star population using 2MASS observations as deep as 1 mag below the nominal survey limit which results in $K_s \sim 16$. Moreover, in their Fig. 1 (*top right*) a partial ring around the galaxy is delineated by sources with $0.5 < J - K_s < 1.5$. However, at their sensitivity and within the above colour range these sources are not C stars but M stars (cf. Fig. 18). Therefore, what Block et al. observed is a ring-like structure traced by the brightest O-rich AGB stars very similar to the old and metal-poor ring shown in Fig. 16. This does not exclude that C stars are present in this region but their colour is redder. In fact recently the authors confirmed spectroscopically 7 C stars with $J - K_s > 2$ which they selected from further near-infrared observations down to $K_s \sim 17$ (Block et al. 2007).

An outer ring dominated by M instead of C stars has implications on the age and metallicity distribution. Bright O-rich AGB stars, especially those brighter than the brightest C star observed, are on average more massive (3−5 $M_\odot$) and younger (∼0.1 Gyr old) than C-rich AGB stars having a mass of 1−3 $M_\odot$ and an age of 0.6−2 Gyr (Cioni et al. 2003; Vassiliadis & Wood 1993). This result supports further the conclusion by Block et al. (2007) that these stars formed recently by gas infall tied to the HI warp. On the other hand, it shows the uncertainty of the Block et al. (2004) technique to characterise the outer halo of galaxies using unresolved stars.

Table 1. Photometry of candidate Long-Period Variables.

α(deg)	δ(deg)	i'	$r-i'$	J	H	K_s
23.914114	31.014139	20.85	1.54	18.60	17.76	17.47
23.915800	30.954123	21.14	0.96	19.07	18.01	17.74
23.917891	31.093290	21.40	0.99	18.99	17.84	17.28
23.933479	31.087179	21.16	2.29	18.45	17.59	17.24
23.937286	31.108717	20.77	1.75	18.51	17.68	17.27
23.948526	31.005262	20.82	1.75	18.47	17.57	17.37
23.952553	31.029049	20.79	0.75	18.89	17.95	17.53
23.964951	31.150126	20.76	1.52	18.09	17.24	16.89
23.786018	31.104441	21.23	1.94	18.71	17.72	17.57
23.786890	31.061749	21.09	1.75	18.99	18.03	17.75
...	...	...	...	...	...	...

Table 2. Combined Spitzer and near-infrared photometry.

SpitzerID	α(deg)	δ(deg)	J	H	K_s
J013201.90 + 302603.3	23.007860	30.434172	18.62	17.45	16.53
J013203.89 + 302507.9	23.016174	30.418797	17.66	17.13	16.87
J013204.84 + 302759.1	23.020119	30.466366	19.35	18.06	16.96
J013206.01 + 302658.2	23.024990	30.449432	18.42	17.16	16.47
J013206.80 + 303843.4	23.028303	30.645323	18.45	17.36	16.65
J013209.90 + 302909.6	23.041250	30.485947	15.59	14.77	14.44
J013210.16 + 304138.9	23.042223	30.694136	18.38	17.34	16.87
J013211.71 + 302059.1	23.048784	30.349678	15.54	14.95	14.84
J013214.11 + 304423.9	23.058659	30.739985	18.44	17.17	16.38
J013214.13 + 302913.7	23.058855	30.487104	17.90	16.88	16.32
...	...	...	...	...	...

The most accurate way to determine age and metallicity of a stellar population is to resolve turn-off main sequence stars. Alternatively, if only much brighter stars are reached, the K_s method, developed by Cioni et al. (2006a) and used here, provides a means to indicate average values as well as investigate relative differences. The next more detailed approach is to fit the observed near-infrared colour magnitude diagrams, dominated by late-type stars, with synthetic diagrams obtained using newly published and continuously improving isochrones (Marigo et al. 2008). Obtaining age and metallicity from unresolved stellar populations may hide non-negligible information about the spatial distribution of these quantities.

4.3. Spitzer variables

Very recently McQuinn et al. (2007) presented the analysis of multi-epoch infrared observations of M 33 using the Spitzer Space Telescope. Figure 18 shows the cross-identified sources between our near-infrared photometry and their Table 3 of variable point sources. We found that out of 2923 Spitzer variables 847 have a near-infrared counterpart within 1″. The histogram of the distance between near-infrared and Spitzer matches has a well defined peak at 0.32″ with a $FWHM = 0.2''$; systematic shifts in both coordinates are ≤0.05″. These obscured variables distribute along the bright half of the branches occupied by O-rich and C-rich AGB stars as well as populating the region of extreme AGB stars (with $(J-K_s)_0 > 2$) and supergiants ($(J-K_s)_0 < 1$). The fact that sources with $(J-K_s)_0 > 2$ are confirmed to vary at infrared wavelengths marks their nature as LPVs, despite the incompleteness of the Hartman et al. (2006) catalogue, supporting further our selection criteria. The table with our near-infrared photometry and the Spitzer photometry by McQuinn et al. (2007), of which an extract is given in Table 2, is available electronically; coordinates are from UKIRT data.

4.4. The C/M ratio and the mean metallicity of the stellar population across M 33

There are essentially two ways to statistically select C-type and M-type AGB stars from photometric observations. In this work we use the $(J-K_s, K_s)$ colour-magnitude diagram (Sect. 3.1) while Rowe et al. (2005) use a colour-colour diagram obtained from the combination of broad-band VI and narrow-band CN-TiO filters (their Fig. 10). The main advantage of the first criterion is that near-infrared observations are not affected by interstellar extinction and produce a more complete sample of stars. In fact, Rowe et al. (2005) observations in the spiral arms suffer from dust extinction which reduces their star counts because faint stars will fall below the detection limit. If the dust extinction is as severe as in the centre of the Milky Way near-infrared observations would suffer a similar effect but this is not the case in M 33. On the other hand, narrow-band observations target those molecular features that are typical of C-type and M-type AGB stars and produce a more reliable selection of stars especially at faint magnitudes where the contamination of RGB stars is stronger.

Rowe et al. (2005) find 7936 C stars but their sample is incomplete towards the centre. Their overall AGB distribution drops at ∼30′ when the contamination by foreground dwarfs becomes severe (see their Fig. 9). Depending on the selection criteria we find 9522/7404 C stars and judging from Fig. 5 the selected AGB stars are almost negligibly affected by foreground stars. A detailed comparison between our C/M ratio distribution (Fig. 10) and the distribution obtained by Rowe et al. (2005, their Fig. 18) confirms that the C/M ratio is high along a ring-like structure surrounding a central region of low ratio. Our observations and analysis reveal a much more complex structure because of the high penetrating power of near-infrared observations which also cover the whole extent of M 33 while Rowe et al. (2005) observations covered only 2/3 of the galaxy. The northern enhancement in the C/M ratio may also correspond to the stellar arc found by Block et al. (2004) but the lack of axis labels in their Fig. 1 makes it hard to secure such a correspondence.

How well does the C/M ratio alone trace metallicity? M 33 presents a metallicity gradient such that the metallicity ([Fe/H]) decreases linearly with galactocentric radius from −0.6 to −0.9 dex (Kim et al. 2002; Barker et al. 2007) although with $[\alpha/\mathrm{Fe}] = 0.0$ the metallicity is 0.4 dex higher (Barker et al. 2007); this gradient extends out to ∼50′ (13 kpc). Brooks et al. (2004) observed a SE halo field and derived a metallicity of $[\mathrm{Fe/H}] = -1.24$ dex while Tiede et al. (2004) and Davidge (2003) in fields approximately in the same direction but closer to the galaxy centre derive $[\mathrm{Fe/H}] = -1.0$ dex. The latter is typical of disc stars rather than halo stars of M 33. Both McConnachie et al. (2006) and Sarajedini et al. (2006) showed that RGB and RR Lyrae stars, respectively, belong to two populations: one associated with the halo ([Fe/H] ∼ −1.4 dex) and the other with the disc ([Fe/H] ∼ −0.8 dex) of M 33. There is a third component in the outer SW region with the same metallicity as the disc which McConnachie et al. (2006) attribute to a stellar stream. The metallicity spread that we obtain from the distribution of the C/M ratio reproduces the spread of the above values and the existing gradient rather well. Both Figs. 10 and 11 show a more detailed structure/substructures than is derived from a gradient

representation of the metallicity. However, we fail to recover a metallicity as high as [Fe/H] = −0.26 dex (Stephens & Frogel 2002) in the nuclear region. According to Mouhcine & Lançon (2003) the C/M ratio traces the metallicity of a population older than about a Gyr. In fact, also across the Magellanic Clouds Cioni et al. (2006a,b) derived that the SFH does affect the C/M if the population is younger than a few Gyr across the LMC while across the Small Magellanic Cloud (SMC) the C/M ratio traces only the intermediate-age epoch of formation of AGB stars. The latter might be influenced by the spatial orientation of the SMC which was not corrected for.

The distribution of metallicity shown in Figs. 15 and 16 has many features in common with the distribution of the C/M ratio shown in Figs. 10 or 11. There is a broad metal-poor outer ring, this metallicity may extend to the whole galaxy if the resolution of the C/M map increases (cf. Figs. 11 and 10) which may explain why the metallicity derived from C stars (Fig. 15) is low in the whole disc. Although the C/M ratio suggests a metallicity which is slightly higher inside a ring-like structure it fails to recover a high metallicity in the centre of the galaxy (see above) which is instead clearly obtained from the analysis of the magnitude distribution of both C and M stars (Figs. 15 and 16). This points to the importance of the age of the stellar population in the interpretation of the C/M ratio distribution which perhaps traces, for this galaxy, only the metallicity at the epoch of formation of AGB stars. On the other hand, an almost flat metallicity gradient has been found by Magrini et al. (2007) from the observation of various elements in a limited sample of young stars, HII regions, PNe and RGB stars. Their results support an evolutionary scenario where M 33 is constantly accreting gas and forming stars at a slowly decreasing rate with time. The rather smooth distribution of metallicity shown in Fig. 15 would agree with this interpretation.

The absolute values of age and metallicity obtained using the K_s method are model dependent and this means that they may be affected by systematic differences. Given that the metallicity in the outer disc of M 33 has been inferred to be ∼1 dex, it means that the value obtained from C stars is off by 0.6 dex. However, if C stars were tracing the halo instead of the disc the derived metallicity would be off by just 0.2 dex. On the contrary, the disc-like metallicity obtained from M stars is too high by 0.5 dex with respect to the expected disc metallicity. The average of the C and M stars would produce the same metallicity obtained by other authors. It is possible that C stars are not just sampling the disc but the halo of the galaxy. It remains unexplained why both C and M stars trace a population with a similar mean age but very different mean metallicities.

4.5. Mean-age of the stellar population across M 33

Focusing on the most significant distributions of mean age obtained from C (Fig. 15-*top*) and M (Fig. 16-*bottom*) stars, M 33 appears overall older than the Magellanic Clouds (Cioni et al. 2006a,b). Here, we compare our results of the mean age distribution with studies in the literature that cover a similar area. This excludes the recent work by Barker et al. (2007) on the outer M 33 regions where they detect an increasing age (from 6 to 8 Gyr) with increasing radius. Our outermost ring-like structure, which does not overlap Barker et al.'s fields, is consistent with a mean age of ∼6 Gyr; perhaps this is the same population connecting to Barker et al.'s inner field. This outer mean age is also in agreement with the results by Li et al. (2004). These authors derived the age distribution across M 33 by comparing observations obtained in several narrow bands from about 350 nm to 1000 nm with synthetic spectral energy distributions produced using the PEGASE code. Although they do not provide enough information on the size of the three regions outlined in their Fig. 4 a comparison with our Fig. 15 shows that, apart from the agreement in the outer region, there is a clear disagreement in the mean age of the inner galaxy. Li et al. (2004) suggest that the central regions are older than the outer regions, except for the spiral arms where the mean age is the youngest. In Fig. 15 the spiral arm region is not distinguishable from the outer region (this is perhaps due to the low resolution imposed by the area subdivision into sectors of rings – Fig. 5) but the difference between Li et al's mean age and our mean age is ∼1 Gyr. On the contrary, both Figs. 15 and 16 suggest a population of a few Gyr younger in the central regions. This result is consistent with the distribution of young stars (super giant stars) confined to the central region almost enclosing the nucleus of the galaxy (Rowe et al. 2005), see also Fig. 4. These authors show that both AGB and main-sequence stars trace the extended structure of M 33 where the latter is clumpier due to localised regions of massive star birth. This cospatial distribution suggests a very similar mean age which supports the smooth outer ring derived in Fig. 15.

5. Conclusions

In this paper we present wide-field near-infrared observations of M 33 obtained with WFCAM at UKIRT. These data reveal a large population of AGB stars which we have used to determine the distribution of age and metallicity across the galaxy as well as to constraint its orientation in the sky.

C-rich and O-rich AGB stars have been selected from the ($J - K_s$, K_s) colour-magnitude diagram using two criteria: one based on a by eye evaluation of their favorite location in the diagram, often used in the literature, and one based on stellar evolutionary tracks. The selection of the two samples is confirmed via the cross-identification with the catalogue of candidate LPVs by Hartman et al. (2006) and with the recent publication of the list of sources detected by Spitzer (McQuinn et al. 2007) in the same region. While the variable sources delineate well the branches populated by un-obscured AGB stars, the latter extend to red colours where stars have thick circumstellar dusty envelope. Both tables containing the cross-identification between our near-infrared photometry and the sample of variable stars and of Spitzer detections are available electronically.

The confirmed location of C-rich and O-rich AGB stars in the near-infrared colour-magnitude diagram has shown that the metal-poor arcs surrounding the galaxy suggested by Block et al. (2004) are formed by O-rich AGB stars, contrary to C-rich AGB stars, and support an LMC-type metallicity as well as an old stellar population. The distribution of the C/M ratio confirms a metallicity gradient corresponding to a spread of [Fe/H] = 0.6 dex and shows substructures in the inner and in the outer parts of the galaxy. A high ratio, or a low metallicity follows the major spiral arms of the galaxy which appears more metal rich in the centre. The peak magnitude and colour of C stars, but also of M stars, describe a sinusoidal pattern which may explain previous inconsistencies on the determination of the distance to the galaxy from sample stars at different locations with respect to the centre, but could also be affected by differential extinction and the disc warp.

We have interpreted the K_s magnitude distribution of both C-type and M-type AGB stars using theoretical distributions constructed from stellar evolution models spanning a range of SFRs and metallicities. This is the same procedure adopted to study the SFH across the Magellanic Clouds (Cioni et al. 2006a,b). Maps showing the distribution of metallicity as a

function of mean age of the stellar population of M 33 indicate a metal poor disc/halo and a metal-rich core as well as metal-rich clumps in the inner part of the galaxy which change location with time. This is perhaps tracing the temporal evolution of the galaxy and suggests that although M 33 is more or less isolated in the sky the star formation proceeded inhomogeneously with time. Contrary to the metallicity value derived from C and M stars which differ by ∼1 dex the distribution of age commonly suggests a broad outer ring ∼6 Gyr old (constant SFR) which surrounds a younger central region, perhaps with the exception of the core which is also metal rich.

Summarizing, this study deconvolves the effect of reddening, structure, metallicity and age on the luminosity function (magnitude distribution in the K_s band) of the stellar population of M 33 as follows. Assuming that near-infrared observations of the M 33 stellar population are negligibly affected by differential reddening, and that there are no variations in age and metallicity for AGB stars in restricted range of colours, their peak magnitude traces distances throughout the extent of the galaxy. Correcting the observed K_s magnitude distribution for this geometrical effect, the fits obtained using theoretical distributions provide the best measurement of mean age and metallicity across the system where relative variations are much more significant than absolute values. By considering the C/M ratio as an independent whilst indirect indicator of metallicity, the most probable star formation rate (or mean age), out of 25 perhaps not realistic simple stellar population templates, is revealed as a function of position within the galaxy.

Despite the strong links of the K_s method to the specific stellar evolutionary models employed and their treatment of the AGB phase, which is still uncertain (Marigo et al. 2008), this method provides a satisfactory approach to the interpretation of variations of age and metallicity across galaxies, complemented by the C/M ratio as an indirect indicator of iron abundance. These studies are particularly important in distant systems where only the brightest stars, e.g. AGB stars, are observed and therefore it is not possible to determine an accurate star formation history and its spatial variations from classic indicators like the main-sequence turn-off.

Acknowledgements. A.M.N.F. and A.H. acknowledge support from a Marie Curie Excellence Grant from the European Commission under contract MCEXT-CT-2005-025869.

References

Barker, M. K., Sarajedini, A., Geisler, D., et al. 2007a, AJ, 133, 1125
Barker, M. K., Sarajedini, A., Geisler, D., et al. 2007b, AJ, 133, 1138
Battinelli, P., & Demers, S. 2005, A&A, 434, 657
Battinelli, P., Demers, S., & Mannucci, F. 2007, A&A, 474, 35
Bellazzini, M., Ferraro, F. R., Sollim, A., et al. 2004, A&A, 424, 199
Bergeat, J., Knapik, A., & Rutili, B. 2001, A&A, 369, 178
Bertelli, G., Bressan, A., Chiosi, C., et al. 1994, A&AS, 106, 275
Block, D. L., Freeman, K. C., Jarret, T. H., et al. 2004, A&A, 425, 37
Block, D. L., Combes, F., Puerari, I., et al. 2007, A&A, 471, 467
Bonanos, A. Z., Stanek, K. Z., Kudritzki, R. P., et al. 2006, ApJ, 652, 313
Brooks, R. S., Wilson, C. D., & Harris, W. E. 2004, AJ, 128, 237
Cioni, M.-R. L., & Habing, H. J. 2003, A&A, 402, 133
Cioni, M.-R. L., & Habing, H. J. 2005, A&A, 429, 837
Cioni, M.-R. L., van der Marel, R. P., Loup, C., & Habing, H. J. 2000, A&A, 359, 601
Cioni, M.-R. L., Marquette, J.-B., Loup, C., et al. 2001, A&A, 377, 945
Cioni, M.-R. L., Blommaert, J. A. D. L., Groenewegen, M. A. T., et al. 2003, A&A, 406, 51
Cioni, M.-R. L., Girardi, L., Marigo, P., & Habing, H. J. 2006a, A&A, 448, 77
Cioni, M-R. L., Girardi, L., Marigo, P., & Habing, H. J. 2006b, A&A, 452, 195
Corbelli, E., & Schneider, S. E. 1997, ApJ, 479, 244
Costa, E., & Frogel, J. A. 1996, AJ, 112, 2607
Davidge, T. J. 2003, AJ, 125, 3046
Galleti, S., Bellazzini, M., & Ferraro, F. R. 2004, A&A, 423, 925
Girardi, L., Bressan, A., Bertelli, G., & Chiosi, C. 2000, A&AS, 141, 371
Girardi, L., Bertelli, G., Bressan, A., et al. 2002, A&A, 391, 195
Girardi, L., Bertelli, G., Chiosi, C., & Marigo, P. 2003, IAUS, 212, 551
Girardi, L., Groenewegen, M. A. T., Hatziminaoglou, E., & da Costa, L. 2005, A&A, 436, 895
Glass, I., & Schultheis, M. 2003, MNRAS, 345, 39
Groenewegen, M. A. T. 2004, A&A, 425, 595
Hartman, J. D., Bersier, D., Stanek, K. Z., et al. 2006, MNRAS, 371, 1405
Hogg, D. W. 2001, AJ, 121, 1207
Kim, M., Kim, E., Lee, M. G., et al. 2002, AJ, 123, 244
Li, J., Ma, J., Zhou, X., et al. 2004, A&A, 420, 89
Magrini, L., Corbelli, E., & Galli, D. 2007, A&A, 470, 843
Marigo, P., & Girardi, L. 2007, A&A, 469, 239
Marigo, P., Girardi, L., & Bressan, A. 1999, A&A, 344, 123
Marigo, P., Girardi, L., & Chiosi, C. 2003, A&A, 403, 225
Marigo, P., Girardi, L., Bressan, A., et al. 2008, A&A, 482, 883
McConnachie, A. W. 2005, Ph.D. Thesis
McConnachie, A. W., Irwin, M. J., Ferguson, A. M. N., et al. 2004, MNRAS, 350, 243
McConnachie, A. W., Alan, W., Chapman, S. C., et al. 2006, ApJ, 647, 25
Mouhcine, M., & Lançon, A. 2003, MNRAS, 338, 572
McLean, I. S., & Liu, T. 1996, ApJ, 456, 499
McQuinn, K. B. W., Woodward, C. E., Willner, S. P., et al. 2007, ApJ, 664, 850
Rowe, J. F., Richer, H. B., Brewer, J. P., & Crabtree, D. R. 2005, AJ, 129, 729
Sarajedini, A., Barker, M. K., Geisler, D., et al. 2006, AJ, 132, 1361
Stephens, A. W., & Frogel, J. A. 2002, AJ, 124, 2023
Tiede, G. P., Sarajedini, A., & Barker, M. K. 2004, AJ, 128, 224
Tokunaga, A. T., Simons, D. A., & Vacca, W. D. 2002, PASP, 114, 180
van den Bergh, S. 2000, in The Galaxies of the Local Group, Cambridge Astr. Ser.
van der Marel, R. P., & Cioni, M.-R. L. 2001, AJ, 122, 1807
Vassiliadis, E., & Wood, P. R. 1993, ApJ, 413, 641
Zaritsky, D., Elston, R., & Hill, M. 1989, AJ, 97, 97